



**The Kinetics of Dimethylhydroxypyridinone Interactions with Iron(III) and the Catalysis of Iron(III) Ligand Exchange Reactions: Implications for Bacterial Iron Transport and Combination Chelation Therapies**

Journal:	<i>Dalton Transactions</i>
Manuscript ID	DT-ART-04-2018-001329
Article Type:	Paper
Date Submitted by the Author:	05-Apr-2018
Complete List of Authors:	Harrington, James; RTI International, Analytical Sciences; Duke University, Chemistry Mysore, Manu; Duke University, Chemistry Crumbliss, Alvin; Duke University, Chemistry

**The Kinetics of Dimethylhydroxypyridinone Interactions with Iron(III) and  
the Catalysis of Iron(III) Ligand Exchange Reactions: Implications for  
Bacterial Iron Transport and Combination Chelation Therapies**

A Full Paper submitted for publication in the journal Metallomics

James M. Harrington,<sup>1,2</sup> Manu M. Mysore,<sup>2</sup> and Alvin L. Crumbliss<sup>2,\*</sup>

<sup>1</sup> RTI International, Research Triangle Park, NC, United States

<sup>2</sup>Department of Chemistry, Duke University, Durham, NC 27708-0346

\* Address correspondence to this author

[alvin.crumbliss@duke.edu](mailto:alvin.crumbliss@duke.edu)

Keywords: Bacterial iron transport, combination chelation therapy, siderophore, kinetics,  
iron(III) ligand exchange, catalysis

## Abstract

Many microbes acquire environmental Fe by secreting organic chelators, siderophores, which possess the characteristics of a high and specific binding affinity for iron(III) that results in the formation of thermodynamically stable, and kinetically inert iron(III) complexes. Mechanisms to overcome the kinetic inertness include the labilization of iron(III) by means of ternary complex formation with small chelators. This study describes a kinetic investigation of the labilization of iron(III) between two stable binding sites, the prototypical siderophore ferrioxamine B and EDTA, by the bidentate siderophore mimic, 1,2-dimethyl-3-hydroxy-4-pyridinone (L1, H(DMHP)). The proposed mechanism is substantiated by investigating the iron(III) exchange reaction between ferrioxamine B and H(DMHP) to form  $\text{Fe}(\text{DMHP})_3$ , as well as the iron(III) exchange from  $\text{Fe}(\text{DMHP})_3$  to EDTA. It is also shown that H(DMHP) is a more effective catalyst for the iron(III) exchange reaction than hydroxamate chelators reported previously, supporting the hypothesis that chelator structure and iron(III) affinity influence low denticity ligand facilitated catalysis of iron(III) exchange reactions. The results are also discussed in the context of the design and use of combination chelator therapies in the treatment of Fe overload in humans.

## Introduction

Iron is essential to the survival and functionality of nearly all living organisms, with the exception of certain lactobacilli and *Borrelia burgdorferi*, the causative agent of Lyme disease.<sup>1</sup> Iron is the fourth most abundant element in the Earth's crust and comprises a large percent of its mass, numbers that are suggestive of its vital importance.<sup>2</sup> However, a delicate balance must be maintained both at a cellular and higher organism level; too much iron can result in toxicity related to iron overload, while too little can cause anemia. For microorganisms, there are two main problems associated with iron uptake. First, its utilization by cells is hindered by the low solubility of the most stable oxidation state in oxic conditions, iron(III). At physiological conditions, iron(III) readily undergoes hydrolysis to form various insoluble products, e.g.  $\text{Fe}_2\text{O}_3$  and  $\text{Fe}(\text{H}_2\text{O})_3(\text{OH})_3$ , which has a solubility product on the order of  $10^{-38}$ .<sup>4</sup> In addition, excess iron can be toxic due to possible redox chemistry with oxygen, superoxide and peroxide that results in the formation of reactive oxygen species (ROS) that can cause extensive damage to cellular components, including the cell wall, DNA, and proteins.<sup>3</sup>

Microorganisms have evolved to address the problem of iron bioavailability through a variety of pathways, one of which is siderophore-mediated iron uptake. This involves the synthesis and release of siderophores, which are small-molecule iron-specific chelators that feature a variety of architectures.<sup>5-12</sup> Siderophores make iron bioavailable both by forming soluble complexes with deep thermodynamic wells and providing a mechanism for specific recognition by receptor proteins at the cell surface, facilitating uptake. Additionally, siderophores protect the cell by limiting the participation of iron in redox reactions through a shift of the redox

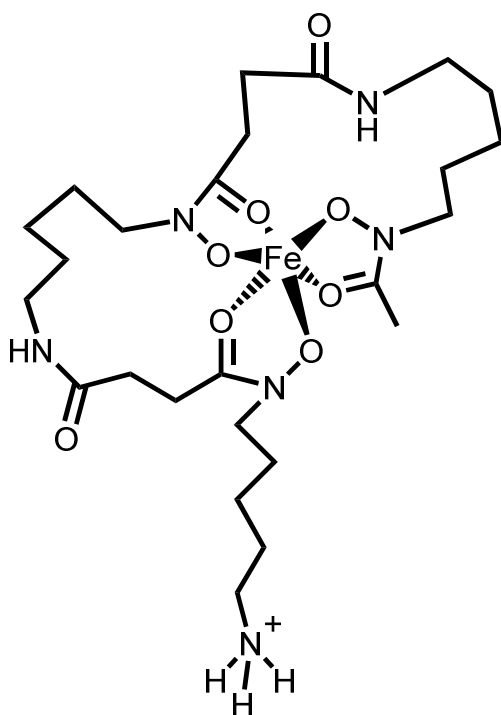
potential of the metal out of the range where it can participate in Fenton chemistry and the Haber-Weiss cycle.<sup>7</sup>

Polydentate siderophores form iron(III) complexes that are generally inert to ligand exchange.<sup>6</sup> An important step in the microbial iron uptake process may involve the exchange of iron between two chelators or a chelator and an iron binding protein. This exchange process is important in certain siderophore-mediated uptake systems such as those of mycobacteria, where membrane-bound siderophores called mycobactins function as a short-term iron storage pool when the iron transport receptors are overwhelmed.<sup>13</sup> The operative reaction that allows mycobactins to function in this way is an exchange reaction of iron(III) from the extracellular siderophores, called exochelins or carboxymycobactins.<sup>14</sup> Chelator exchange reactions are also of importance in other pathogens, where the siderophores produced by the bacterium remove iron from the host iron chelators such as transferrin to sequester it for assimilation and use.<sup>15</sup>

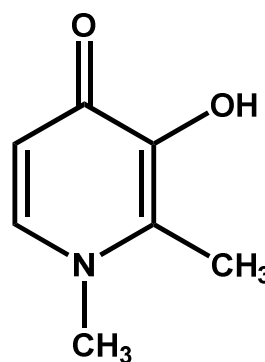
Some biologically relevant iron exchange reactions have been shown to be influenced by the presence of secondary chelating agents capable of ternary complex formation.<sup>5</sup> A previous study showed that secondary chelators that have a high affinity for iron(II) can affect the redox potential of iron(III)-siderophore complexes; for example, it was shown that the presence of bathophenanthroline disulfonate, a secondary chelator with a specific affinity for iron(II) will facilitate reduction of iron(III) in the ferrioxamine B complex by ascorbate and glutathione.<sup>16</sup> Another study showed that the presence of secondary chelators results in acceleration of the exchange of iron(III) from ferrioxamine B to another hexadentate chelator, EDTA, by a non-redox mechanism.<sup>17</sup> Addition of hydroxamic acid chelators to the exchange reaction resulted in acceleration of the observed rate of reaction. It has also been shown that small organic chelators

can affect the dissolution of minerals synergistically in the presence of siderophores.<sup>18</sup> Chloride anion will also catalyze Fe(III) exchange between polydentate chelates through ternary complex formation.<sup>19</sup>

Our current study was designed with two purposes in mind. First, as a continuation of our long term interest in mechanisms for catalyzing the exchange of Fe(III) between polydentate ligands of high binding affinity that are relevant to microbial iron acquisition pathways.<sup>5, 9, 17, 19</sup> Consequently, we have investigated the exchange of Fe(III) between ferrioxamine B (**I**) and EDTA in the presence of 1,2-dimethyl-3-hydroxy-4-pyridinone (**II**), a low mw bidentate ligand



Ferrioxamine B  
Fe(HDFB)<sup>+</sup>  
**I**



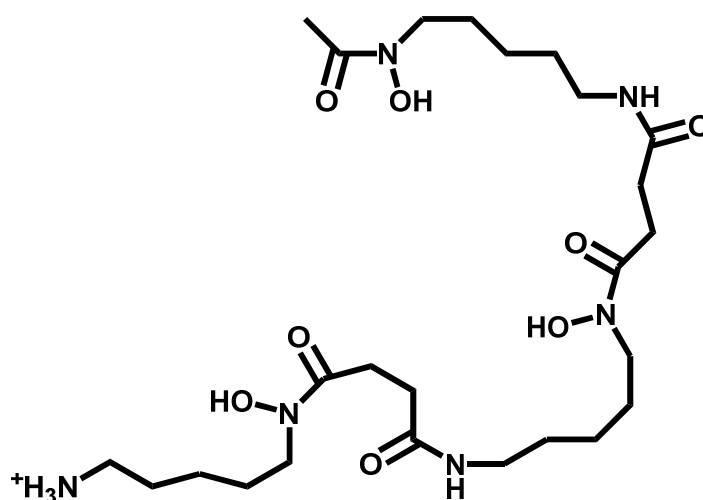
1,2-dimethyl-3-hydroxy-4-pyridinone  
H(DMHP)  
Ferriprox®, L1, Deferiprone  
**II**

&lt;DMHP catalysis paper submitted 1-26-18.docx&gt;

which may potentially serve as a Fe(III)-ligand exchange catalyst. Second, iron chelation is an important therapy for the treatment of iron overload associated with repeated blood transfusions necessitated by  $\beta$ -thalassaemia major, sickle cell anemia, and neurodegenerative diseases. Our selection of ferrioxamine B and H(DMHP) specifically for this study was dictated by recent interest in chelator combination therapies for the treatment of iron overload diseases.

Combination therapy is an attempt to enhance iron excretion from the patient by using a low mw bidentate chelator capable of cell membrane penetration, in combination with a polydentate chelator of high thermodynamic affinity for Fe(III), and presumably low kinetic lability.<sup>20-24</sup>

Desferrioxamine B (**III**), a natural siderophore produced by *Streptomyces pilosus* for iron



Desferrioxamine B  
H<sub>4</sub>DFB<sup>+</sup>  
Desferal®  
**III**

acquisition necessary for growth is marketed by Novartis in the mesylate salt form as a drug, Desferal<sup>®</sup>, used widely in the treatment of iron overload and is FDA approved for use in the United States. Unfortunately, Desferal has poor oral absorption and must be administered by

parenteral infusion, making treatments long and uncomfortable for patients, which can in turn result in decreased patient compliance rates. H(DMHP) (also referred to in the early medicinal chemistry literature as L1) is marketed by Apotex, Inc as an orally active drug, Ferriprox<sup>®</sup>, for iron removal from overloaded patients and is approved for use in the EU, Canada, and the United States. H(DMHP) in combination with desferrioxamine B has been reported to enhance non transferrin-bound iron (NTBI) removal from patients.<sup>24</sup>

Here we have investigated the mechanism of any synergistic interactions between ferrioxamine B and H(DMHP) in the presence of a thermodynamic Fe(III) sink (excess EDTA) under controlled conditions *in vitro*. Kinetic lability of desferrioxamine B bound Fe(III) may result in redistribution of the excess iron *in vivo*, producing toxicity associated with combination therapy regimes. Results presented here suggest that caution should be used in designing combination therapeutic iron chelation regimes. In principle, a smaller, kinetically labile bidentate chelator can rapidly access intracellular Fe pools. While it has been shown *in vivo* that H(DMHP) can shuttle Fe from transferrin to desferrioxamine B,<sup>20</sup> the shuttle can work both ways; i.e. the labilization of Fe(III) bound to desferrioxamine B. The mechanism for labilization of siderophore bound Fe(III) presented here also has application to *in vivo* microbial iron acquisition pathways.

## Experimental

### Materials

All solutions were prepared in deionized water. A solution of 0.10 M NaClO<sub>4</sub> (99.99%, Sigma Aldrich, St. Louis, MO) with 0.20 M sodium acetate (>99%, Sigma Aldrich) was used as the background electrolyte for solution pH values ranging from 4.0 to 5.5 and 0.20 M MES

&lt;DMHP catalysis paper submitted 1-26-18.docx&gt;

Buffer (>99.5%, Sigma Aldrich) was used at solution pH values ranging from 5.5 to 6.0. Acetate buffer solution pH values were adjusted with 1.0 M HClO<sub>4</sub>. The minimum volume of acid necessary to adjust the pH was used to minimize the effect on solution ionic strength, which was held constant at 0.1 M. Solid NaOH was used to adjust the pH value of MES buffer solutions to minimize the change in ionic strength. Solid anhydrous Fe(ClO<sub>4</sub>)<sub>3</sub> (99.9+%, Sigma) was used to prepare a stock solution in 0.10 M HClO<sub>4</sub>. The stock solution was standardized titrimetrically by reduction with SnCl<sub>2</sub>, followed by titration with K<sub>2</sub>Cr<sub>2</sub>O<sub>7</sub>.<sup>25</sup> Stock EDTA solutions were prepared with solid EDTA (99+%, Acros Organics, Belgium) dissolved in the acetate buffered background electrolyte. Desferrioxamine B mesylate (>92.5%) and 1,2-dimethyl-3-hydroxy-4-pyridinone (H(DMHP), 98%) were obtained from Sigma-Aldrich and used as received to prepare stock solutions. Solutions of ferrioxamine B were prepared by gradual addition with stirring of Fe(ClO<sub>4</sub>)<sub>3</sub> stock solution to an unbuffered solution of desferrioxamine B mesylate, followed by dilution to volume with the buffered electrolyte background to a final concentration of 100 mM acetate buffer. A stock solution of Fe(DMHP)<sub>3</sub> was prepared similarly by slow addition with stirring of iron stock solution to an unbuffered solution of H(DMHP), followed by dilution to volume with the buffered electrolyte. All stock solutions of ligands were prepared similarly to maintain buffer concentration.

All pH measurements were made with an Orion 230 A+ pH/ion meter equipped with an Orion Ross pH electrode filled with 3 M NaCl solution. The electrode was calibrated by titration of standardized 0.10 M HCl with standardized 0.10 M NaOH, as in the “classical method,” and calibration data were analyzed using the computer program, GLEE.<sup>26</sup>

### **Kinetic measurements**

All kinetic measurements were made under pseudo first order conditions. Absorption spectra were recorded as a function of time over the wavelength range 300 to 650 nm using a Varian-Cary 50 or 100 spectrophotometer with temperature control at 25 °C. The absorbance over time at a fixed wavelength was fit to a single exponential decay model, shown in Eq. (1), where  $A$  represents the absorbance at time  $t$ ,  $m$  represents the amplitude of the

$$A = me^{-k_{\text{obs}}t} + A_{\text{inf}} \quad (1)$$

absorbance change,  $k_{\text{obs}}$  represents the observed rate constant for the first-order reaction, and  $A_{\text{inf}}$  represents the final absorbance. In each experiment, data were analyzed at four different wavelengths with equivalent results.

### **Iron(III) exchange from ferrioxamine B to EDTA in the absence and presence of**

**H(DMHP).** A series of experiments at various EDTA and H(DMHP) concentrations were performed using stock solutions of 3 mM ferrioxamine B, 30 mM EDTA, and 31 mM

H(DMHP). The iron(III) exchange reaction was initiated by rapid addition of the ferrioxamine B solution to a solution containing various concentrations of EDTA and H(DMHP). Kinetic data were obtained under pseudo-first-order conditions with respect to EDTA over a range of EDTA concentrations from 5 mM to 15 mM. At each EDTA concentration, the concentration of H(DMHP) was varied over the range of 0 to 5 mM. The final concentration of ferrioxamine B complex in all experiments was 0.4 mM at a final pH of 4.35 (100 mM NaOAc buffer).

**Iron(III) exchange from ferrioxamine B to H(DMHP).** Iron(III) exchange reactions were performed between ferrioxamine B and H(DMHP) under similar conditions as the reactions in

&lt;DMHP catalysis paper submitted 1-26-18.docx&gt;

the presence of EDTA. Solutions were mixed to produce final concentrations of 0.2 mM ferrioxamine B and a range of H(DMHP) concentrations from 4 mM to 10 mM at pH 4.35 (100 mM NaOAc buffer). Reactions were monitored until the spectrum was constant with respect to time. The final spectrum was compared to expected absorbance values determined from literature reports of the molar absorptivity of the Fe(DMHP)<sub>3</sub> complex to verify the product.<sup>27</sup> The reactions were repeated over a range of pH values. The solution pH was varied by changing the buffer system. The experiments were repeated in 100 mM NaOAc/100 mM NaClO<sub>4</sub> buffer at and below pH 4.61, and in 100 mM MES/100 mM NaClO<sub>4</sub> buffer at pH 4.85, pH 5.50, and pH 6.00.

**Iron(III) exchange from Fe(DMHP)<sub>3</sub> to EDTA.** The exchange of iron(III) from Fe(DMHP)<sub>3</sub> to EDTA was performed in a similar manner as the ferrioxamine B - H(DMHP) exchange reaction. Solutions of 0.4 mM iron(III) with 4 mM H(DMHP) and 0.4 mM iron(III) with 10 mM H(DMHP) were prepared in acetate-buffered background electrolyte and reacted with a range of EDTA solutions with concentrations from 4 to 20 mM. The solutions were mixed in a 1:1 ratio and the reaction was monitored spectrophotometrically over the range of 325 to 650 nm until the solution spectrum was constant. The identity of the final product was verified by comparison to the known solution spectra of Fe(EDTA) and other known Fe complexes.<sup>28</sup>

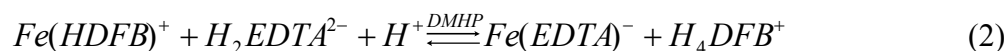
### Speciation plots

Iron(III) complex speciation plots were generated using the speciation simulation program HySS.<sup>29</sup>

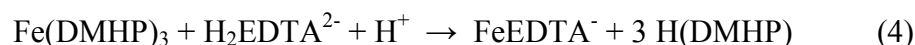
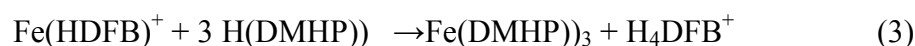
## Results and Discussion

## Overview

The iron(III) exchange reaction from ferrioxamine B (**I**) to EDTA is slow, as the reaction involves exchange of the metal between two thermodynamically stable hexadentate chelate complexes that are kinetically inert. We observed, however, that addition of H(DMHP) (**II**) accelerates the iron(III) exchange reaction shown in Reaction (2). Mechanistic information relevant to Reaction (2) was obtained by studying the reaction as a function of EDTA, H(DMHP), and  $H^+$



concentrations, and by investigating the iron(III) exchange reaction between ferrioxamine B and H(DMHP) (Reaction (3)), and between  $Fe(DMHP)_3$  and EDTA (Reaction (4)).



## Kinetics of iron(III) exchange from ferrioxamine B to EDTA (Reaction (2))

The iron(III) exchange reaction in the absence of added H(DMHP) (Reaction (2);  $[H(DMHP)] = 0$ ) takes place over the course of 2-5 hours at  $pH = 4.35$  and  $25\text{ }^\circ\text{C}$ , depending on the concentration of EDTA. Representative time dependent spectra are shown in Fig. S1 (Supporting Information) and the absorbance measured at a single wavelength as a function of time is shown in Fig. S2. The clean isosbestic point and fit to a single exponential decay model is consistent with a pseudo first order reaction (excess EDTA) with the rate law shown in Eq. (5).

&lt;DMHP catalysis paper submitted 1-26-18.docx&gt;

$$\text{Rate} = k_{\text{obs}}[\text{Fe}(\text{HDFB})^+] \quad (5)$$

Figure 1, shows a linear relationship (curve A) between  $k_{\text{obs}}$  and [EDTA] (Eq. (6)) for the uncatalyzed Reaction (2) ( $[\text{H}(\text{DMHP})] = 0$ ).

$$k_{\text{obs}} = k_1[\text{EDTA}] \quad (6)$$

The second order rate constant  $k_1 = 0.030 \text{ M}^{-1}\text{s}^{-1}$  (Table 1) was obtained from the slope for curve A in Fig. 1. This value is consistent with a previous report for Reaction (2) at similar conditions.<sup>17</sup>

Time resolved spectral changes for Reaction. (2) in the presence of H(DMHP) (Fig. S3) are consistent with those observed in the absence of H(DMHP) (Fig. S1), suggesting that the initial reactant and product species are the same in both cases. A single wavelength absorbance decay model that is representative of four different wavelengths is presented in Fig S4. The rate constants determined at all four wavelengths were equivalent within experimental error, consistent with the presence of an isosbestic point and suggesting that no stable intermediate is present during Reaction (2) in the presence of H(DMHP).

The observed pseudo-first-order rate constants for Reaction (2) were plotted as a function of H(DMHP) concentration for five different EDTA concentrations (Fig. S5), and as a function of EDTA concentration at five different H(DMHP) concentrations (Fig. 1). Analysis of these data allows us to write the rate law in Eq. (7) for Reaction (2) (see Supporting Information for derivation details and independent determinations of  $k_2$  and  $k_3$ ).

$$\text{Rate} = k_{\text{obs}}[\text{FeHDFB}^+] = \{k_2[\text{H}(\text{DMHP})] + k_3[\text{EDTA}]\}[\text{FeHDFB}^+] \quad (7)$$

As discussed in Supporting Information within the derivation of Eq. (7), evidence of the internal consistency of our data set may be obtained by comparing values for  $k_2$  obtained from the slopes of the plots in Fig. S5 ( $k_2 = 1.12(9) \text{ M}^{-1}\text{s}^{-1}$ ) with the value obtained from the y-intercepts of the plots in Fig. 1 ( $k_2 = 1.0(1) \text{ M}^{-1}\text{s}^{-1}$ ). In a further internal consistency comparison, the rate constants obtained from kinetic data for the direct reaction of EDTA with ferrioxamine B in the absence of H(DMHP) ( $k_1 = 0.03(8) \text{ M}^{-1}\text{s}^{-1}$ ) and in the presence of [H(DMHP)] from the intercepts of  $k_{\text{obs}}$  vs [H(DMHP)] plots (Fig. S5;  $k_3 = 0.028(5) \text{ M}^{-1}\text{s}^{-1}$ ), and from the slopes of the plots in Fig. 1 ( $k_3 = 0.06 \text{ M}^{-1}\text{s}^{-1}$ ) are in reasonable agreement. (Comparison of the rate constant values obtained from Fig. 1 gives a closer comparison with the results for Reaction (2) in the absence of H(DMHP) ( $k_3 = 0.028(5) \text{ M}^{-1}\text{s}^{-1}$ ) with higher precision than the values obtained from Fig. S5.) This confirms interpretation of  $k_3$  in Eq. (7) as the rate constant for direct attack of EDTA on Ferrioxamine B. These results are summarized in Table 1.

While it would be desirable to compare the rate constants for the iron(III) exchange reaction from ferrioxamine B to EDTA in the presence of H(DMHP) over a range of pH values, speciation plots for this system suggest that at high H(DMHP) concentrations, H(DMHP) and desferrioxamine B can out-compete EDTA for iron sequestration (Fig. S6). Consequently, the pH dependence of the reaction of H(DMHP) with  $\text{FeHDFB}^+$  was investigated only for Reaction (3) as described below.

### **Kinetics of iron(III) exchange from ferrioxamine B to H(DMHP) (Reaction (3))**

The spectra measured during the iron(III) exchange reaction of ferrioxamine B with H(DMHP) (Reaction (3)) are shown in Fig. S7 and support the identity of the reaction product as

&lt;DMHP catalysis paper submitted 1-26-18.docx&gt;

Fe(DMHP)<sub>3</sub> ( $\lambda_{\text{max}} = 457 \text{ nm}$ ), suggesting complete conversion of the FeHDFB<sup>+</sup> complex to Fe(DMHP)<sub>3</sub> at our conditions.<sup>27</sup> The absorbance change measured at a single wavelength (Fig. S8) can be fit with a single exponential decay model (Eq. (1)), consistent with a single kinetically observable rate-limiting step, as well as confirming first-order dependence of the rate law on FeHDFB<sup>+</sup> concentration. The observed pseudo first-order rate constants yielded a linear plot as a function of H(DMHP) concentration from 4 to 10 mM (Fig. 2; squares), consistent with first-order dependence of the rate on H(DMHP) concentration. This suggests the involvement of one equivalent of H(DMHP) in the rate-determining step of the reaction and establishes Eq. (8) as the

$$\text{Rate} = k_{\text{obs}}[\text{FeHDFB}^+] = k_4[\text{H(DMHP)}][\text{FeHDFB}^+] \quad (8)$$

rate law for Reaction (3). The second order rate constant ( $k_4 = 1.13(9) \text{ M}^{-1} \text{ s}^{-1}$ ) may be obtained from the slope of the plot in Fig. 2 (squares). The y-intercepts of the plots in Fig. 1 also provide observed pseudo first-order rate constants for the reaction of ferrioxamine B with H(DMHP) (Reaction (3)). Fig. 2 (diamonds) includes these rate constants, illustrating the internal consistency of our data set. The slopes of the lines in Fig. 2, representing the second order rate constant ( $k_4$ ) for Reaction (3), are comparable within experimental error ( $0.96 \pm 0.03 \text{ M}^{-1} \text{ s}^{-1}$  for the data diamonds) extrapolated from Reaction (2) and  $1.13 \pm 0.09 \text{ M}^{-1} \text{ s}^{-1}$  for the experimental data (squares) from Reaction (3)). Due to this agreement, we propose that Reactions (2) and (3) proceed by the same rate determining step, which will be discussed later.

Additional experiments were performed for Reaction (3) over the range of pH values from 4.35 to 6.00 to determine if there is a  $[\text{H}^+]$  dependence on  $k_4$ . All experiments could be fit to a single exponential decay model with similar spectral shifts, suggesting that the reactions proceed by the same mechanism at all pH values investigated. Plots of  $k_{\text{obs}}$  for Reaction (3) as a

function of H(DMHP) concentration at various fixed  $[H^+]$  are shown in Fig. 3. The slopes of the lines in Fig. 3, representing the second order rate constant  $k_4$  for Reaction (3), vary with  $[H^+]$  as shown in Fig. 4. The plot in Fig. 4 suggests a linear relationship (Eq. (9)) where  $k_5$  and  $k_6$  are obtained from the slope and intercept respectively.

$$k_4 = k_5[H^+] + k_6 \quad (9)$$

This observation indicates the presence of two parallel pathways for Reaction (3) that are described by the rate law shown in Eqs. (10) and (11):

$$\text{Rate} = (k_5[H^+] + k_6)[H(\text{DMHP})][\text{FeHDFB}^+] \quad (10)$$

$$\text{Rate} = k_5[H^+][H(\text{DMHP})\text{FeHDFB}^+] + k_6[H(\text{DMHP})][\text{FeHDFB}^+] \quad (11)$$

The values of  $k_5$  and  $k_6$  determined from the slope and intercept of Fig. 4 are listed in Table 1. A  $k_4$  value calculated from Eq. (9) when the pH = 4.35 is  $0.71 \text{ M}^{-1}\text{s}^{-1}$ , in reasonable agreement with  $k_4$  obtained from the slope of the plot in Fig. 2, illustrating the internal consistency of our interpretation of the data set.

### **Kinetics of iron(III) exchange from H(DMHP) to EDTA (Reaction (4))**

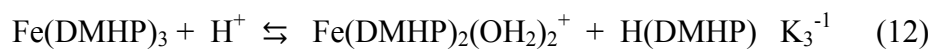
Representative time dependent spectra for exchange Reaction (4) are shown in Fig. S9 and absorbance changes at a single wavelength are illustrated in Fig. S10. A single exponential decay model at four independent wavelengths produced equivalent results, suggesting that a single reaction was observable during the exchange process and that the rate law is first-order with respect to  $\text{Fe}(\text{DMHP})_3$  complex concentration. Observed pseudo first-order rate constants obtained in the presence of two different excess H(DMHP) concentrations plotted as a function

&lt;DMHP catalysis paper submitted 1-26-18.docx&gt;

of EDTA concentration yielded linear relationships (Fig. S11), suggesting that Reaction (4) is first-order with respect to EDTA. The plots exhibited zero y-intercepts at both H(DMHP) concentrations, suggesting no appreciable back reaction of the  $\text{Fe}(\text{EDTA})^-$  complex with H(DMHP) at our conditions. The slopes at different H(DMHP) concentrations suggest an inverse dependence of the reaction rate on H(DMHP) concentration.

To explore the inverse dependence of the reaction rate on H(DMHP) concentration, a series of experiments was performed by varying the concentration of H(DMHP) present in solution at a constant EDTA concentration. A plot of the observed pseudo first-order rate constant as a function of H(DMHP) concentration, which illustrates this inverse relationship, is shown in Fig. 5.

Inverse first order dependence of the observed pseudo first order rate constant on  $[\text{H}(\text{DMHP})]$  for Reaction (4) may be accommodated by considering a rapid reversible pre-equilibrium reaction to produce the reactive species  $\text{Fe}(\text{DMHP})_2(\text{OH}_2)_2^+$  (Reaction (12)), followed by reaction with EDTA in the rate determining step (Reaction (13)).



The rate law for such a two-step process takes the form shown in Eq. (14)

$$\text{Rate} = k_7[\text{EDTA}][\text{Fe}(\text{DMHP})_2(\text{OH}_2)_2^+] \quad (14)$$

Since the  $[\text{Fe}(\text{DMHP})_2(\text{H}_2\text{O})_2^+]$  concentration is low in the presence of excess  $\text{H}(\text{DMHP})$  and since in measuring pseudo-first-order rate constants we are observing the rate of disappearance of  $\text{Fe}(\text{DMHP})_3$  according to Eq. (15),

$$\text{Rate} = k_{\text{obs}}[\text{Fe}(\text{DMHP})_3] \quad (15)$$

rate expression (14) may be transformed to Eq. (16) as described in Supporting Information.

$$\text{Rate} = k_7[\text{EDTA}][\text{Fe}(\text{DMHP})_3][\text{H}^+] / (K_3[\text{H}(\text{DMHP})]) \quad (16)$$

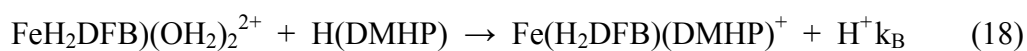
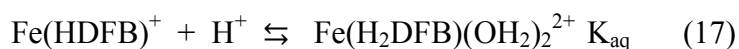
Through analysis of the data from three independent data sets shown in Fig. 5 and Fig. S11 as detailed in Supporting Information, we obtain an internally consistent value of  $3.4 \times 10^2 \text{ M}^{-1}\text{s}^{-1}$  for  $k_7$ , the second order rate constant in Eq. (14) for Reaction (4) (Table 1).

### Mechanistic analysis

The exchange of iron(III) from ferrioxamine B to EDTA is accelerated by the presence of  $\text{H}(\text{DMHP})$  (Reaction (2)). The observed two-term rate Equation (7) for Reaction (2) is consistent with a parallel path mechanism for the  $\text{Fe}(\text{III})$  exchange reaction where the  $[\text{H}(\text{DMHP})]$  dependent path is responsible for the catalytic effect of  $\text{H}(\text{DMHP})$  in producing  $\text{Fe}(\text{EDTA})^-$ . A comparison of  $k_2$  and  $k_3$  values experimentally obtained demonstrates a 20-fold rate acceleration for  $\text{Fe}(\text{III})$  exchange from ferrioxamine B to EDTA in the presence of  $\text{H}(\text{DMHP})$  at pH 4.35. Kinetic data and time dependent spectra for Reaction (3) respond to the question: what is the nature of the  $\text{H}(\text{DMHP})$  catalytic path in Reaction (2)? Specifically, what is the rate determining step, and the structure and lifetime of any intermediates along the reaction coordinate? The equivalent values for the experimentally observed macroscopic second-order rate constants  $k_2$  and  $k_4$  (Table 1) for Reaction (2) and Reaction (3) respectively, suggest that these reactions have the same rate determining steps and transition state structures. Kinetic data

and time dependent spectra for Reaction (4) confirm that  $\text{Fe}(\text{DMHP})_3$  is not formed as an intermediate in Reactions (2) or (3), and thus suggests that the structure of the reactive intermediate is  $\text{Fe}(\text{H}_2\text{DFB})(\text{DMHP})^+$ . Further, this catalytically active species is short lived as Reactions (2) and (3) proceed with the maintenance of an isosbestic point. This means that any intermediates formed, such as  $\text{Fe}(\text{H}_2\text{DFB})(\text{DMHP})^+$ , have only a transient existence at low concentration, or their spectra in this region strongly resemble reactants or products. The latter case is unlikely, given published spectra of  $\text{Fe}(\text{HDFB})^+$ ,  $\text{FeEDTA}^-$  and  $\text{Fe}(\text{III})$  complexes of  $\text{H}(\text{DMHP})$ .<sup>5, 30</sup> The subsequent question is: what is the rate determining step in the formation of the intermediate  $\text{Fe}(\text{H}_2\text{DFB})(\text{DMHP})^+$ ? The details of this mechanistic analysis are as follows.

The macroscopic rate constants for the  $[\text{H}(\text{DMHP})]$  dependent path in Reaction (2) ( $k_2 = 1.1 \text{ M}^{-1}\text{s}^{-1}$ ) and Reaction (3) ( $k_4 = 1.1 \text{ M}^{-1}\text{s}^{-1}$ ) are equivalent at pH 4.35. This and the fact that both rate laws are first order in  $[\text{H}(\text{DMHP})]$  suggest that the rate determining step involves the formation of the ternary complex  $\text{Fe}(\text{H}_2\text{DFB})(\text{DMHP})^+$ . Considering the pH dependence observed for Reaction (3), we propose the following mechanism for the formation of  $\text{Fe}(\text{H}_2\text{DFB})(\text{DMHP})^+$  in Reactions (2) and (3).



Reaction (17) cannot be the rate determining step as this reaction is known to be rapid<sup>31</sup> and furthermore the rate laws for Reactions (2) and (3) exhibit first order dependence on  $[\text{H}(\text{DMHP})]$  concentration. Treating Reaction (17) as a rapidly established pre-equilibrium with  $K = 10^{0.94}$ <sup>32</sup> and Reaction (18) as the rate determining step, the rate law for the formation of  $\text{Fe}(\text{H}_2\text{DFB})(\text{DMHP})^+$  via Reactions (2) and (3) is as follows (see Supporting Information for a derivation of Eq. (19)):

$$\text{Rate} = k_B K_{aq} [H^+] [H(\text{DMHP})] [\text{Fe}(\text{HDFB})^+] \quad (19)$$

where  $K_{aq}$  is the equilibrium constant for the dissociation of a terminal hydroxamate moiety for ferrioxamine B in Reaction (17) and  $k_B$  is the bimolecular rate constant for Reaction (18).

Equation (20) relates the experimentally observed macroscopic rate constants  $k_2$  and  $k_4$

$$k_2 \approx k_4 = k_B K_{aq} [H^+] \quad (20)$$

to the microscopic constants  $k_B$  and  $K_{aq}$  in Eq. (19). Assuming the common value  $1.1 \text{ M}^{-1}\text{s}^{-1}$  for  $k_2$  and  $k_4$  and  $[H^+] = 10^{-4.35} \text{ M}$  we obtain  $k_B = 2.3 \times 10^3 \text{ M}^{-1}\text{s}^{-1}$  for the second order rate constant for Reaction (18). This result is in excellent agreement with literature values for aquo ligand substitution in iron(III) - diaquo and tetraquo complexes  $\text{Fe}(\text{L})_4(\text{OH}_2)_2^{n+}$  and  $\text{Fe}(\text{L})_2(\text{OH}_2)_4^{n+}$  where the second order rate constants are in the range of  $10^3 \text{ M}^{-1}\text{s}^{-1}$ .<sup>5, 33, 34</sup> Treating Reaction (18) as the attack of an  $(\text{DMHP})^-$  anion on  $\text{Fe}(\text{H}_2\text{DFB})(\text{OH}_2)_2^{2+}$  results in a calculated value of  $k_B = 8 \times 10^8 \text{ M}^{-1}\text{s}^{-1}$  which is several orders of magnitude too high for aqua ligand substitution in  $\text{Fe}(\text{H}_2\text{DFB})(\text{OH}_2)_2^{2+}$ .<sup>33</sup> Furthermore, this would not be consistent with the observed  $[H^+]$  dependence for Reaction (3).

When we consider Eq. (20) in the context of Eq. (9) and rate expression Eq. (11) for the pH dependence of Reaction (3) we have

$$k_B K_{aq} [H^+] = k_5 [H^+] + k_6 = 1.1 \text{ M}^{-1}\text{s}^{-1} \text{ at pH } 4.35 \quad (21)$$

As noted above  $k_B = 2.3 \times 10^3 \text{ M}^{-1} \text{ s}^{-1}$  at pH 4.35 where

$$k_B = \{ k_5 [H^+] + k_6 \} / K_{aq} [H^+] \quad (22)$$

Alternatively, from our pH dependent analysis of Reaction (3) we have that

$$k_2 \approx k_4 = k_5 [H^+] + k_6 = 1.1 \text{ M}^{-1}\text{s}^{-1} \quad (23)$$

so that

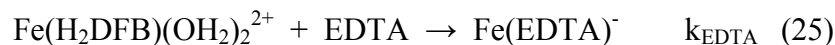
$$k_B = 1.1 / K_{aq} [H^+] = 2.8 \times 10^3 \text{ M}^{-1} \text{ s}^{-1} \text{ at pH } = 4.35 \quad (24)$$

&lt;DMHP catalysis paper submitted 1-26-18.docx&gt;

This excellent agreement in Eqs. (22 and (24) demonstrates the internal consistency of our data and the validity of our mechanistic interpretation.

Our analysis of the kinetics of Reaction (4) establishes that  $\text{Fe}(\text{DMHP})_3$  is not a transient or transition state in Reaction (2), since we do not observe any inverse dependence on  $[\text{H}(\text{DMHP})]$  in our kinetic data. That is, the observed increase in rate with  $[\text{H}(\text{DMHP})]$  in Reaction (2) should eventually level off or decrease if  $\text{Fe}(\text{DMHP})_3$  or  $\text{Fe}(\text{DMHP})_2(\text{OH}_2)_2^+$  were present along the reaction coordinate. Consequently we are left with the conclusion that  $\text{Fe}(\text{H}_2\text{DFB})(\text{DMHP})^+$  is formed as the reactive intermediate in the rate determining step in Reaction (2) and in Reaction (3).

For Reaction (2) we also propose the reaction of EDTA with  $\text{Fe}(\text{H}_2\text{DFB})(\text{OH}_2)_2^{2+}$  for the  $[\text{H}(\text{DMHP})]$  independent non-catalyzed path. In this case



$$k_1 = k_3 = k_{\text{EDTA}}K_{\text{aq}}[\text{H}^+] \quad (26)$$

where  $k_3 = 3 \times 10^{-2} \text{ M}^{-1}\text{s}^{-1}$  at pH 4.35 which yields  $k_{\text{EDTA}} = 7.7 \times 10^1 \text{ M}^{-1}\text{s}^{-1}$ . This is significantly less than the attack of  $\text{H}(\text{DMHP})$  on  $\text{Fe}(\text{H}_2\text{DFB})(\text{OH}_2)_2^{2+}$  ( $k_{\text{B}} = 2.3 \times 10^3 \text{ M}^{-1}\text{s}^{-1}$ ;  $k_{\text{B}}/k_{\text{EDTA}} = 30$ ) possibly for steric reasons and suggests steric accessibility as another reason for the catalytic effect of  $\text{H}(\text{DMHP})$  on the exchange of  $\text{Fe}(\text{III})$  between ferrioxamine B and EDTA.

A summary of the overall reaction scheme, the interrelationships between Reactions (2), (3) and (4), and the microscopic rate constants derived from our kinetic data are presented in Scheme 1.

To determine the  $H^+$  source for protonation of the dissociated hydroxamate donor group in Reaction (2) and Reaction (3), it was necessary to investigate the rate of reaction over a range of pH values. This reveals the pH dependence of the reaction and can provide information about the overall mechanism of iron(III) exchange in both Reactions (2) and (3). While it would be desirable to compare the rate constants of the iron(III) exchange reaction from ferrioxamine B to EDTA in the presence of H(DMHP) over a range of pH values, speciation plots for this system suggest that at high H(DMHP) concentrations, H(DMHP) and desferrioxamine B would be able to out-compete EDTA for iron chelation (Fig. S6). Since Reaction (3) proceeds through the same reactive intermediate ( $Fe(H_2DFB)(OH_2)_2^{2+}$ ) as Reaction (2), and as there is less chance for undesirable side reactions to occur in Reaction (3), Reaction (3) was chosen as the model for Reactions (2) and (3) for experiments carried out over a range of pH values.

The second order rate constant for Reaction (3) was observed to increase with increasing  $H^+$  concentration (Fig. 4). It is likely that this increase in rate of reaction is due to a shift in the pre-equilibrium Reaction (17) to produce more of the reactive species  $Fe(H_2DFB)(OH_2)_2^{2+}$ . This observation suggests that as the  $H^+$  concentration increases, a rapid increase in the second order rate constant of the reaction will be observed until a very high  $H^+$  concentration, where the maximum rate of reaction is the rate of water ligand/solvent exchange for  $Fe(H_2DFB)(H_2O)_2^{2+}$ . In  $Fe(H_2DFB)(H_2O)_2^{2+}$ , dissociation of the water molecules is much more rapid than that of the hydroxamate donor group in the hexadentate  $Fe(HDFB)^+$  complex.

Equation (11) shows that there are two pathways for Reaction (3) by which iron exchange can occur ( $H^+$  ion-dependent and  $H^+$  ion-independent). The relative importance of both pathways can be calculated from values for the rate constants shown in Table 1. By using the determined rate constants ( $k_5 = 1.1 \times 10^4 \pm 1.3 \times 10^3 \text{ M}^{-2} \text{ s}^{-1}$  and  $k_6 = 2.2 \times 10^{-1} \pm 6.5 \times 10^{-2} \text{ M}^{-1} \text{ s}^{-1}$ ) and

&lt;DMHP catalysis paper submitted 1-26-18.docx&gt;

setting the equations for the parallel pathways equal to each other, it can be shown that the hydrogen ion dependent and hydrogen ion independent pathways are equally efficient at pH 4.72. At higher pHs, the hydrogen ion independent pathway is predominant. Protonation of the dissociating bidentate hydroxamate moiety of the  $\text{FeHDFB}^+$  in the acid independent path likely occurs through  $\text{H}^+$  transfer from the entering  $\text{H}(\text{DMHP})$  to the dissociating hydroxamate moiety as their  $\text{pK}_a$  values are similar.<sup>23, 32</sup> This reaction then allows  $\text{H}(\text{DMHP})$  to enter the inner coordination sphere of the ferrioxamine B complex. This initial intermediate,  $\text{Fe}(\text{H}_2\text{DFB})(\text{DMHP})^{2+}$  is what pushes the reaction to completion. In the context of Reaction (2), protonation of a ferrioxamine B hydroxamate group allows for  $\text{H}(\text{DMHP})$  to enter the first coordination shell of  $\text{Fe}(\text{III})$ , preventing ferrioxamine B ring closure and providing a reactive site for EDTA to exchange with ferrioxamine B (Scheme 1).

A previous study showed that addition of the monohydroxamic acids acetohydroxamic acid, benzylhydroxamic acid, and N-methylacetohydroxamic acid to Reaction (2) would accelerate the exchange of iron(III) from ferrioxamine B to EDTA, and that the mechanism of catalysis was through the formation of a ternary complex.<sup>17</sup> It was also shown that the acceleration of the exchange of iron(III) from ferrioxamine B to EDTA was dependent on the structure of the ternary chelator, such that reactions featuring N-methylacetohydroxamic acid as the catalyst were the most rapid and those featuring acetohydroxamic acid were the least rapid. In all three cases, a significant acceleration of the reaction was only observed at the higher concentrations of ternary ligand (at least 0.10 M).  $\text{H}(\text{DMHP})$  is a more efficient catalyst than the monohydroxamic acids; at 10 mM bidentate chelator concentrations  $\text{H}(\text{DMHP})$  is 100 times more efficient a catalyst than the monohydroxamic acids previously reported. This may be due to the high affinity of  $\text{H}(\text{DMHP})$  for  $\text{Fe}(\text{III})$ . The  $\text{Fe}(\text{III})$   $\log \beta_{110}$  value for  $\text{H}(\text{DMHP})$  is 15.1,

much greater than for N-methylacetohydroxamic acid, 11.70.<sup>27,34</sup> The greater catalytic ability of H(DMHP) compared to the hydroxamic acids may be related to electronic structural characteristics of the ternary chelator. H(DMHP) features a conjugated ring system as part of the donor group, which would result in delocalization of electron density and perhaps increased ternary complex reactivity.

## Conclusions

Metal ion exchange reactions are important in a variety of bio-systems where specific chelators bind to metals. The exchange of iron between two hexadentate chelators is normally a slow reaction at physiological conditions, requiring some driving force to allow the exchange to occur in a biological time frame. In some cases, small molecule metal binding secondary metabolites may be able to promote the exchange reaction. We have shown here that the model small molecule chelator, H(DMHP) can act as a catalyst for the exchange of iron from ferrioxamine B to EDTA. The mechanism of catalysis has been shown to take place through the formation of an inner sphere ternary complex, whereby H(DMHP) traps the reactive  $\text{Fe}(\text{H}_2\text{DFB})(\text{OH}_2)_2^{2+}$  intermediate, thus accelerating the dissociation of the hexadentate desferrioxamine B. This model demonstrates one possible route that organisms may use to obtain iron from environmental siderophore complexes.

While the catalytic effect of H(DMHP) on the exchange of Fe(III) between  $\text{Fe}(\text{HDFB})^+$  and EDTA is relatively modest ( $k_B / k_{\text{EDTA}} \sim 30$ ) the efficiency of this additional path to  $\text{FeEDTA}^-$  product is dependent on H(DMHP) concentration and relatively high H(DMHP) concentrations at low EDTA concentration can significantly accelerate the reaction. This illustrates the potential use of low MW metal binding metabolites in a biological system in

&lt;DMHP catalysis paper submitted 1-26-18.docx&gt;

labilizing Fe(III) bound in a low free energy well and inserted into another stable binding site. This further illustrates the interplay between kinetic lability and tight binding sites in biological metal trafficking.

Returning to the use of combined chelation therapy for iron overloaded patients, work reported here re-emphasizes that reaction catalysis works in both directions. While a small low mw bidentate ligand may be more efficient than hexadentate desferrioxamine B in removing Fe(III) from transferrin or the NTBI pool, it can also remove Fe(III) from the presumed therapeutic agent desferrioxamine B (Desferal<sup>®</sup>), which is viewed as a thermodynamically stable and kinetically inert complex. However, the kinetically inert characterization refers to the complete dissociation of the desferrioxamine B ligand. As demonstrated previously, dissociation of a single hydroxamate unit from ferrioxamine B to form  $\text{Fe}(\text{HDFB})(\text{OH}_2)_2^{2+}$  is labile.<sup>31</sup> As demonstrated here H(DMHP) can readily trap  $\text{Fe}(\text{HDFB})(\text{OH}_2)_2^{2+}$  leading to facile release of Fe(III) from its thermodynamically stable ferrioxamine B complex. Consequently, the design of bidentate/hexadentate combined chelation strategies should take the observed phenomenon into account to mitigate the risk of redistribution of iron in the body. Previous studies have demonstrated in animal models that such “shuttling” of iron occurs during simultaneous DFB/DMHP combination chelation therapy, which has led to the adoption of sequential combination therapy, entailing administration of DFB and DMHP at different times of the day.<sup>35,</sup>

36

### **Conflict of Interest Statement**

The authors of this manuscript would like to declare no conflict of interest, financial or otherwise, related to the work presented here.

**Acknowledgements**

We thank Ting Yu for collecting some of the early data for this project. The National Science Foundation (CHE 0809466), North Carolina Local Section of the American Chemical Society, and Duke University Center for Biomolecular and Tissue Engineering are gratefully acknowledged for financial support of this research. We would also like to acknowledge Dr. Claire Parker Siburt for her collaboration with MMM and Dr. Robert Hider for a helpful discussion.

## Figures

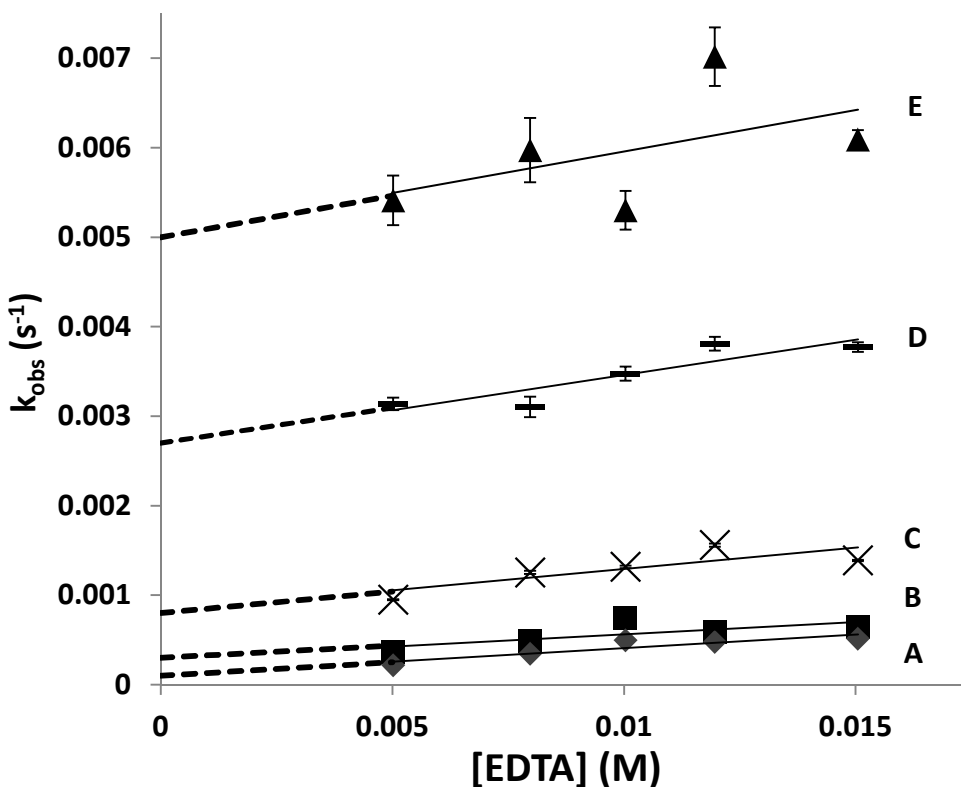


**Figure 1.** Plot of pseudo-first order rate constant,  $k_{\text{obs}}$  as a function of [EDTA] concentration for Reaction (2) at each of five H(DMHP) concentrations. The lines represent the linear best fit plots of  $k_{\text{obs}}$  as a function of [EDTA]. The error bars on data points represent the standard deviation of the average observed rate constants measured at 4 discrete wavelengths in a single experiment. If an error bar is not visible, it is smaller than the data point. All reactions were performed at  $[\text{FeHDFB}^+] = 0.4 \text{ mM}$ ,  $[\text{EDTA}] = 5\text{-}15 \text{ mM}$ ,  $\mu = 0.10 \text{ M}$  ( $\text{NaClO}_4$ ),  $\text{pH} = 4.35$  (100 mM NaOAc buffer), and  $T = 25 \text{ }^\circ\text{C}$ . Legend: **A**  $[\text{H}(\text{DMHP})] = 0 \text{ mM}$ ; **B**  $[\text{H}(\text{DMHP})] = 0.25 \text{ mM}$ ; **C**  $[\text{H}(\text{DMHP})] = 1.0 \text{ mM}$ ; **D**  $[\text{H}(\text{DMHP})] = 2.5 \text{ mM}$ ; **E**  $[\text{H}(\text{DMHP})] = 5.0 \text{ mM}$ . The average slope for the five plots is  $0.06 (2) \text{ M}^{-1} \text{ s}^{-1}$ .

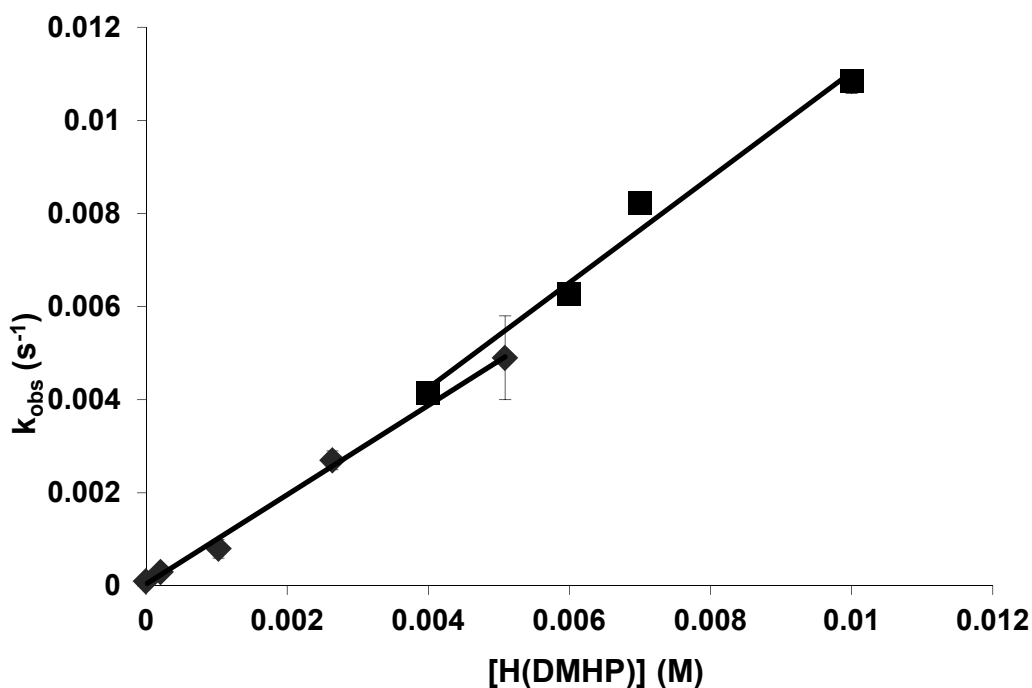


**Figure 2.** Upper line (squares) is a plot of the observed pseudo-first order rate constants for the iron(III) exchange reaction between ferrioxamine B and H(DMHP) (Reaction (3)) as a function of H(DMHP) concentration. Conditions:  $[\text{FeHDFB}^+] = 0.4 \text{ mM}$ ,  $\mu = 0.10 \text{ M}$  ( $\text{NaClO}_4$ ),  $\text{pH} = 4.35$  (100 mM NaOAc buffer), and  $T = 25 \text{ }^\circ\text{C}$ . The lower line (diamonds) is a plot of the pseudo-first-order-rate constants obtained from an extrapolation of the plots in Fig. 1 to  $[\text{EDTA}] = 0$  at different  $[\text{H(DMHP)}]$  concentrations. Conditions:  $[\text{FeHDFB}^+] = 0.4 \text{ mM}$ ,  $\mu = 0.10 \text{ M}$  ( $\text{NaClO}_4$ ),  $\text{pH} = 4.35$  (100 mM NaOAc buffer), and  $T = 25 \text{ }^\circ\text{C}$ . Error bars for the diamonds represent the standard deviation of the y-intercepts of the plots in Fig. 1. Error bars for the squares represent the standard deviation of the average observed rate constant measured at 4 wavelengths in a single experiment. If error bars are not visible, they are smaller than the data point symbols.

&lt;DMHP catalysis paper submitted 1-26-18.docx&gt;

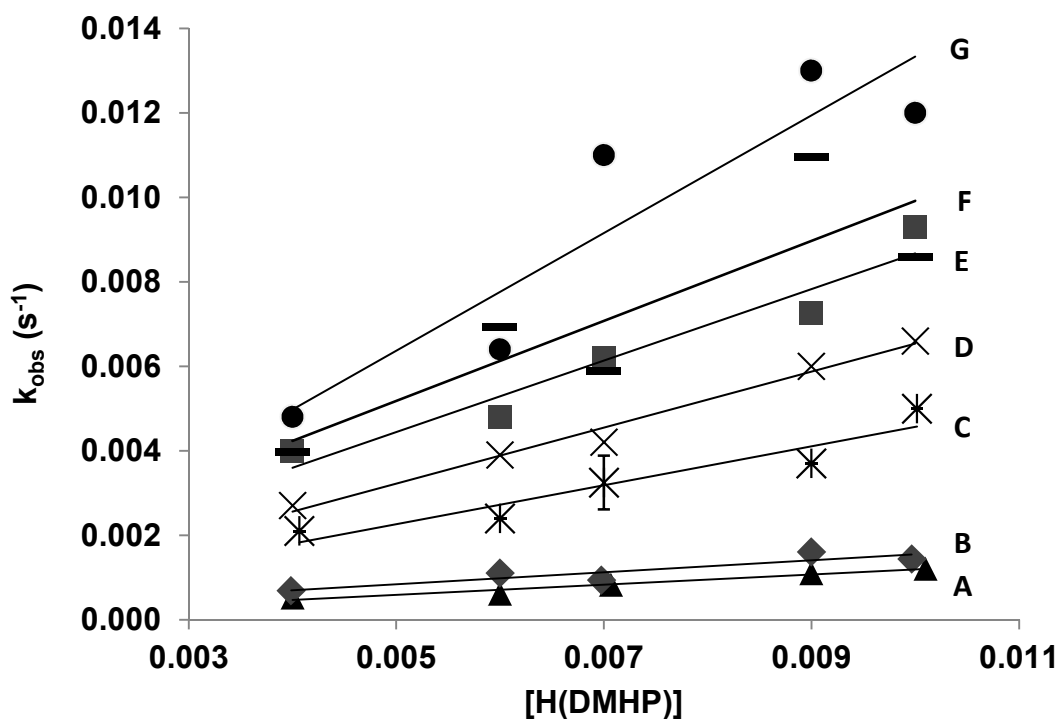


**Figure 3.** Plots of observed pseudo-first order rate constants for the iron(III) exchange reaction between ferrioxamine B and H(DMHP) (Reaction (3)) as a function of H(DMHP) concentration at five pH values. Legend: **A** pH 6.00, **B** pH 5.50, **C** pH 4.85, **D** pH 4.61, **E** pH 4.35, **F** pH 4.15, **G** pH 3.98. Error bars represent the standard deviation of the average observed rate constant measured at 4 discrete wavelengths in a single experiment. If error bars are not visible, they are smaller than the data symbols. Conditions:  $[\text{Fe}^{3+}] = [\text{H}_4\text{DFB}^+] = 0.40 \text{ mM}$ ,  $\mu = 0.10 \text{ M}$  ( $\text{NaClO}_4$ ), and buffer concentration was 100 mM. For experiments performed at and below pH 4.61, the buffer was sodium acetate, and for experiments at pH 4.85, pH 5.50, and pH 6.00, the buffer was MES.

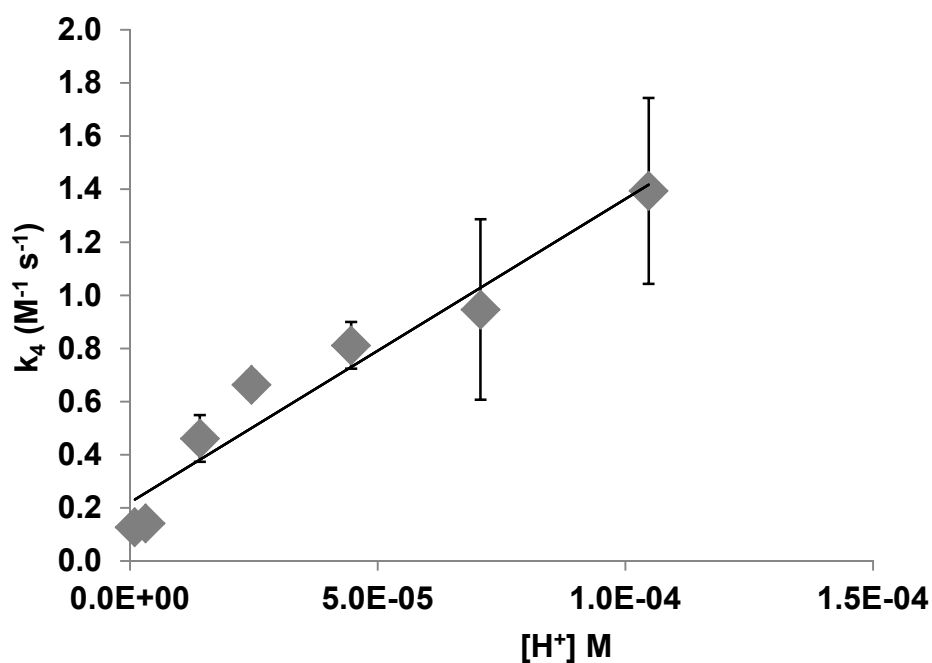


**Figure 4.** Plot of the second order rate constant  $k_4$  for the iron(III) exchange reaction between ferrioxamine B and H(DMHP) (Reaction (3)) as a function of  $[H^+]$ . The solid line represents a fit of Eq. (9) to the data. Error bars represent the standard deviation of the second order rate constant. If error bars are not visible, they are smaller than the data point symbols. Conditions:  $[FeHDFB^+] = 0.4$  mM,  $[H(DMHP)] = 4.0 - 10.0$  mM, and  $T = 25^\circ C$ .

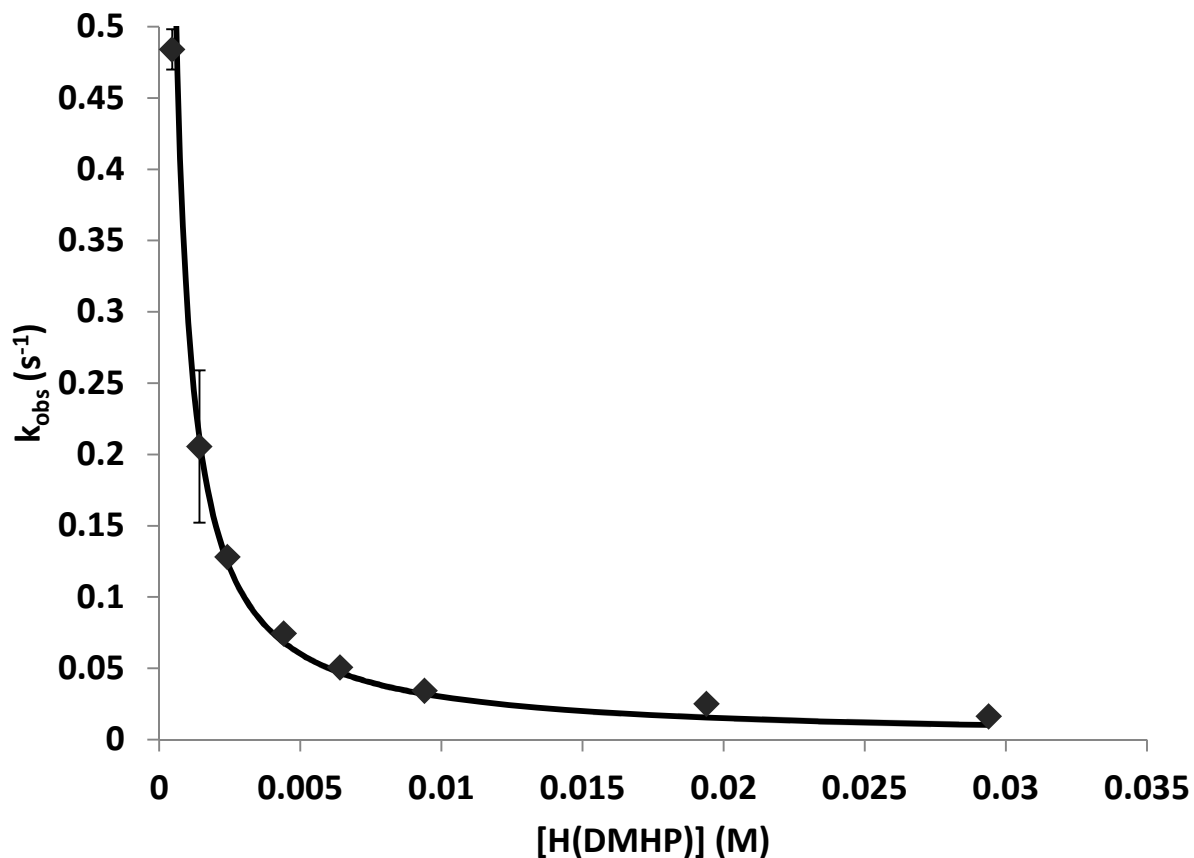


**Figure 5.** Plot of observed pseudo-first-order rate constant for the iron(III) exchange reaction between H(DMHP) and EDTA (Reaction (4)) as a function of the free H(DMHP) concentration. The line represents the best fit of adjustable parameter  $a$  in the equation  $k_{\text{obs}} = a / [\text{H(DMHP)}]_{\text{eq}}$  (see Eq. (S14) in Supporting Information; excluding the data point at 1 mM H(DMHP)), where  $a$  is  $3.01 \times 10^{-4} \text{ Ms}^{-1}$ . Error bars represent the standard deviation of the average observed rate constant measured at 4 discrete wavelengths in a single experiment. Conditions:  $[\text{Fe}^{3+}]_{\text{tot}} = 2.0 \times 10^{-4} \text{ M}$ ,  $[\text{EDTA}] = 6.0 \text{ mM}$ ,  $25.0 \text{ }^\circ\text{C}$ ,  $\text{pH} = 4.35$ ,  $\mu = 0.10 \text{ M}$  ( $\text{NaClO}_4$ ).

## Tables

**Table 1.** Rate constants for the Fe<sup>3+</sup>-HDFB-DMHP-EDTA exchange reactions.

Reaction/Equation	Symbol	Constant <sup>a</sup>
(2) $\text{Fe}(\text{HDFB})^+ + \text{H}_2\text{EDTA}^{2-} + \text{H}^+ \rightleftharpoons \text{Fe}(\text{EDTA})^- + \text{H}_4\text{DFB}^+$	$k_1$	0.030 (8) $\text{M}^{-1} \text{s}^{-1}$ <sup>b</sup>
(5)/(6) Rate = $k_1[\text{EDTA}][\text{Fe}(\text{HDFB})^+]$		
(2) $\text{Fe}(\text{HDFB})^+ + \text{H}_2\text{EDTA}^{2-} + \text{H}^+ \xrightleftharpoons{\text{DMHP}} \text{Fe}(\text{EDTA})^- + \text{H}_4\text{DFB}^+$	$k_2$	1.12 (9) $\text{M}^{-1} \text{s}^{-1}$ <sup>c</sup>
(7) Rate = { $k_2[\text{H}(\text{DMHP})] + k_3[\text{EDTA}]$ } $[\text{Fe}(\text{HDFB})^+]$	$k_2$	1.0 (1) $\text{M}^{-1} \text{s}^{-1}$ <sup>d</sup>
	$k_3$	0.06 (2) $\text{M}^{-1} \text{s}^{-1}$ <sup>e</sup>
	$k_3$	0.028 (5) $\text{M}^{-1} \text{s}^{-1}$ <sup>f</sup>
(3) $\text{Fe}(\text{HDFB})^+ + 3 \text{H}(\text{DMHP}) \rightleftharpoons \text{Fe}(\text{DMHP})_3 + \text{H}_4\text{DFB}^+$	$k_4$	1.13 (9) $\text{M}^{-1} \text{s}^{-1}$ <sup>g</sup>
(8) Rate = $k_4[\text{H}(\text{DMHP})][\text{Fe}(\text{HDFB})^+]$	$k_4$	0.96 (3) $\text{M}^{-1} \text{s}^{-1}$ <sup>h</sup>
(11) Rate = $k_5[\text{H}^+][\text{DMHP}][\text{FeHDFB}^+] + k_6[\text{DMHP}][\text{FeHDFB}^+]$	$k_5$	1.1 (1) $\times 10^4 \text{M}^{-2} \text{s}^{-1}$ <sup>i</sup>
	$k_6$	0.22 (6) $\text{M}^{-1} \text{s}^{-1}$ <sup>j</sup>
(4) $\text{Fe}(\text{DMHP})_3 + \text{H}_2\text{EDTA}^{2-} + \text{H}^+ \rightleftharpoons \text{FeEDTA}^- + 3 \text{H}(\text{DMHP})$	$k_7$	3.4 (1) $\times 10^2 \text{M}^{-1} \text{s}^{-1}$ <sup>k</sup>
(16) Rate = $k_7[\text{EDTA}][\text{Fe}(\text{DMHP})_3][\text{H}^+] / (K_3[\text{H}(\text{DMHP})])$		

<sup>a</sup> Values in parentheses are standard deviations of the last digit. Conditions: T = 25 °C,  $\mu = 0.10 \text{M}$  (NaClO<sub>4</sub>), pH = 4.35.

<sup>b</sup> Value obtained from the slope of the plots shown in Fig. 1.

<sup>c</sup> Value obtained from the average of the slopes of the plots shown in Fig. S5.

<sup>d</sup> Value obtained from the y-intercepts of the plots shown in Fig. 1.

<sup>e</sup> Value obtained from the average of the slopes of the plots shown in Fig. 1.

<sup>f</sup> Value obtained from the y-intercepts of the plots shown in Fig. S5.

<sup>g</sup> Value obtained from the slope of the plot (squares) shown in Fig. 2.

<sup>h</sup> Value obtained from the slope of the plot of intercepts from Fig. 1 and shown in Fig. 2 (diamonds).

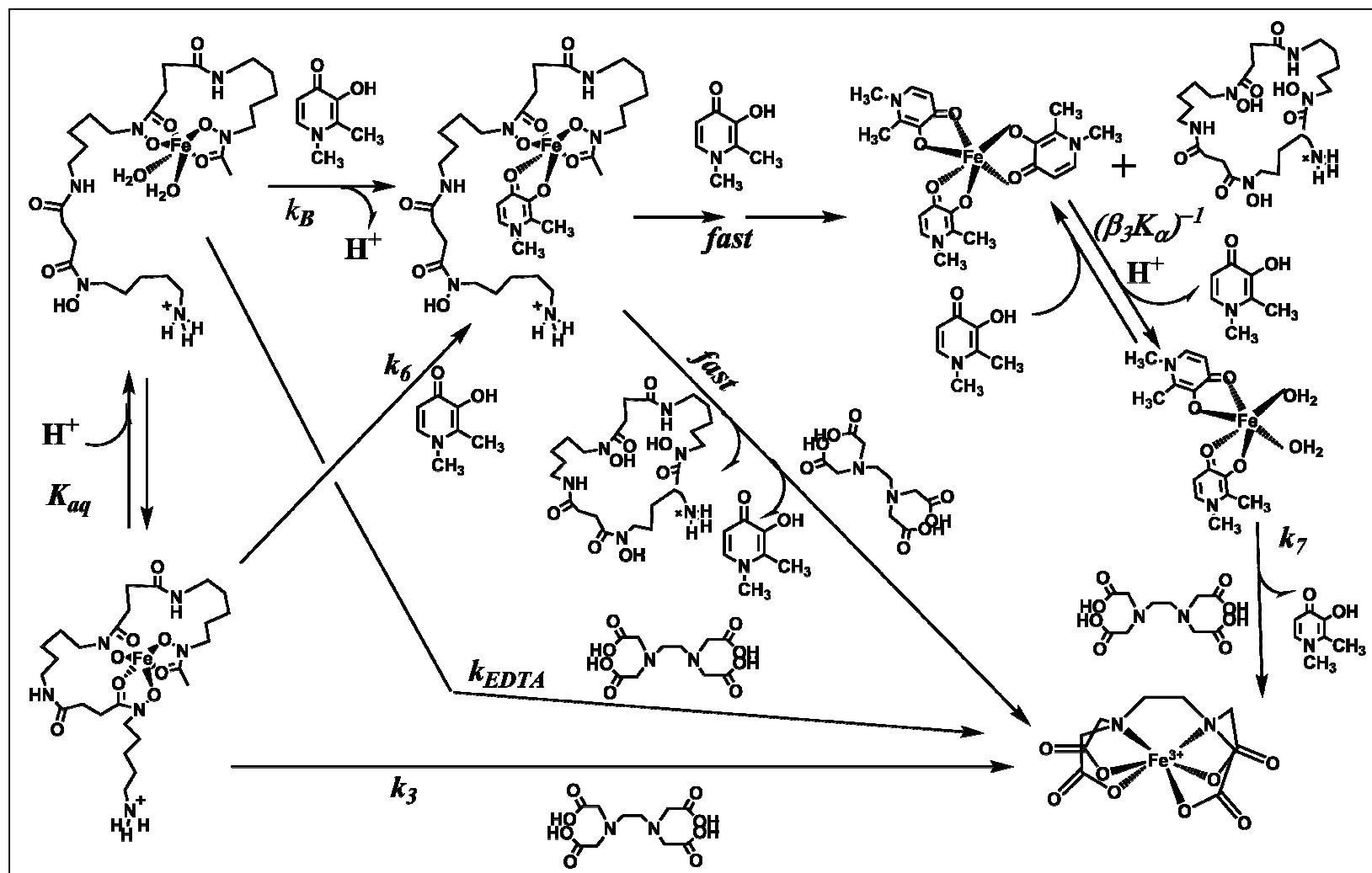
<sup>i</sup> Value obtained from the slope of the plot shown in Fig. 4.

<sup>j</sup> Value obtained from the y-intercept of the plot shown in Fig. 4.

<sup>k</sup> Value obtained from the best fit line shown in Fig. 5 and the slopes of the plots shown in Fig. S11.

&lt;DMHP catalysis paper submitted 1-26-18.docx&gt;

**Scheme 1.** Overall reaction scheme for the exchange of Fe(III) from FeHDFB<sup>+</sup> to EDTA in the presence and absence of H(DMHP). The microscopic rate and equilibrium constants derived from the macroscopic constants determined in the Results section (Table 1) are as defined in the text.  $K_{aq} = 10^{0.94}$ <sup>32</sup>;  $k_B = 2.3 \times 10^3 \text{ M}^{-1} \text{ s}^{-1}$ ;  $(\beta_3 K_a)^{-1} = ((10^{9.24})(10^{-9.76}))^{-1} = 3.31$ <sup>28</sup>;  $k_7 = 3.4 \times 10^2 \text{ M}^{-1} \text{ s}^{-1}$ ;  $k_{EDTA} = 77 \text{ M}^{-1} \text{ s}^{-1}$ ;  $k_6 = 0.22 \text{ M}^{-1} \text{ s}^{-1}$ .



## References

1. F. Archibald, *Lactobacillus plantarum*, an organism not requiring iron, *FEMS microbiology letters*, 1983, **19**, 29-32.
2. J. E. Posey and F. C. Gherardini, Lack of a role for iron in the Lyme disease pathogen, *Science*, 2000, **288**, 1651-1653.
3. R. R. Crichton, in *Biological Inorganic Chemistry*, Elsevier, Amsterdam, 2008, pp. 211-240.
4. C. F. Baes and R. E. Mesmer, *Hydrolysis of cations*, Wiley, 1976.
5. A. M. Albrecht-Gary and A. L. Crumbliss, in *Metal Ions in Biological Systems*, eds. A. Sigel and H. Sigel, M. Dekker, New York, 1998, vol. 35, pp. 239-327.
6. A. L. Crumbliss and J. M. Harrington, in *Adv. Inorg. Chem.*, eds. R. van Eldik and C. D. Hubbard, 2009, vol. 64, pp. 179-250.
7. S. Dhungana and A. L. Crumbliss, Coordination Chemistry and Redox Processes in Siderophore-Mediated Iron Transport *Geomicrobiol. J.*, 2005, **22**, 87.
8. R. C. Hider and X. Kong, Chemistry and biology of siderophores, *Natural product reports*, 2010, **27**, 637-657.
9. K. N. Raymond and E. A. Dertz, Biochemical and physical properties of siderophores, *Iron transport in bacteria*. ASM Press, Washington, DC, 2004, 3-17.
10. R. Saha, N. Saha, R. S. Donofrio and L. L. Bestervelt, Microbial siderophores: a mini review, *Journal of basic microbiology*, 2013, **53**, 303-317.
11. S. D. Springer and A. Butler, Microbial ligand coordination: consideration of biological significance, *Coordination Chemistry Reviews*, 2016, **306**, 628-635.

&lt;DMHP catalysis paper submitted 1-26-18.docx&gt;

12. C. Wandersman and P. Delepelaire, Bacterial iron sources: from siderophores to hemophores, *Annu. Rev. Microbiol.*, 2004, **58**, 611-647.
13. J. M. Harrington, H. Park, Y. Ying, J. Hong and A. L. Crumbliss, Characterization of Fe(III) sequestration by an analog of the cytotoxic siderophore brasilibactin A: Implications for the iron transport mechanism in mycobacteria, *Metallomics*, 2011, **3**, 464-471.
14. C. Ratledge, Iron, mycobacteria and tuberculosis, *Tuberculosis*, 2004, **84**, 110-130.
15. J. E. Anderson, P. F. Sparling and C. N. Cornelissen, Gonococcal transferrin-binding protein 2 facilitates but is not essential for transferrin utilization, *Journal of bacteriology*, 1994, **176**, 3162-3170.
16. K. A. Mies, J. I. Wirgau and A. L. Crumbliss, Ternary Complex Formation Facilitates a Redox Mechanism for Iron Release from a Siderophore, *Biometals*, 2006, **19**, 115.
17. B. F. Monzyk and A. L. Crumbliss, Factors that Influence Siderophore-mediated Iron Bioavailability: Catalysis of Interligand Iron(III) Transfer from Ferrioxamine B to EDTA by Hydroxamic Acids, *J. Inorg. Biochem.*, 1983, **19**, 19-39.
18. L. B. Saal and O. W. Duckworth, Synergistic Dissolution of Manganese Oxides as Promoted by Siderophores and Small Organic Acids, *Soil Sci. Soc. Am. J.*, 2010, **74**, 1513-1529.
19. H. Boukhalfa and A. L. Crumbliss, Kinetics and Mechanism of a Catalytic Chloride Ion Effect on the Dissociation of Model Siderophore Hydroxamate– Iron (III) Complexes, *Inorganic chemistry*, 2001, **40**, 4183-4190.

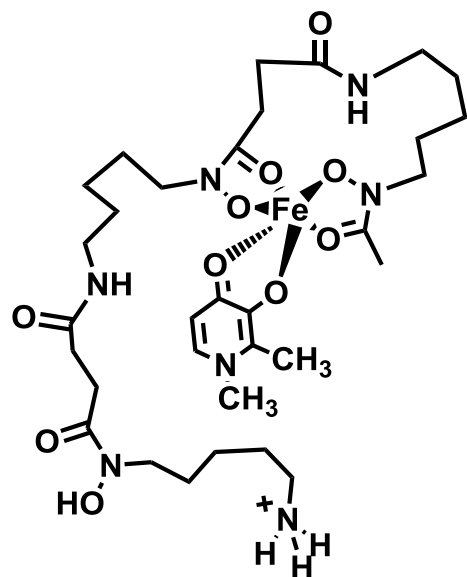
20. L. D. Devanur, R. W. Evans, P. J. Evans and R. C. Hider, Chelator-facilitated removal of iron from transferrin: relevance to combined chelation therapy, *Biochemical Journal*, 2008, **409**, 439-447.
21. R. Galanello, A. Agus, S. Campus, F. Danjou, P. J. Giardina and R. W. Grady, Combined iron chelation therapy, *Annals of the New York Academy of Sciences*, 2010, **1202**, 79-86.
22. Y. Ma, T. Zhou, X. Kong and R. C. Hider, Chelating agents for the treatment of systemic iron overload, *Current medicinal chemistry*, 2012, **19**, 2816-2827.
23. T. Zhou, Y. Ma, X. Kong and R. C. Hider, Design of iron chelators with therapeutic application, *Dalton transactions*, 2012, **41**, 6371-6389.
24. P. Evans, R. Kayyali, R. C. Hider, J. Eccleston and J. B. Porter, Mechanisms for the shuttling of plasma non-transferrin-bound iron (NTBI) onto deferoxamine by deferiprone, *Translational Research*, 2010, **156**, 55-67.
25. A. I. Vogel, *A Text-Book of Quantitative Inorganic Analysis*, Longmans, Green, and Co Ltd, London, 3rd edn., 1961.
26. P. Gans and B. O'Sullivan, GLEE, a new computer program for glass electrode calibration, *Talanta*, 2000, **51**, 33-37.
27. R. J. Motekaitis and A. E. Martell, Stabilities of the iron(III) chelates of 1,2-dimethyl-3-hydroxy-4-pyridinone and related ligands, *Inorg. Chim. Acta*, 1991, **183**, 71.
28. C. Bull, G. J. McClune and J. A. Fee, The Mechanism of Iron EDTA Catalyzed Superoxide Dismutation, *J. Am. Chem. Soc.*, 1983, **105**, 5290.
29. L. Alderighi, P. Gans, A. Ienco, D. Peters, A. Sabatini and A. Vacca, Hyperquad simulation and speciation (HySS): a utility program for the investigation of equilibria

- involving soluble and partially soluble species, *Coordination Chemistry Reviews*, 1999, **184**, 311-318.
30. R. C. Scarrow, Riley, P. E., Abu-Dari, K., White, D. L., Raymond, K. N., Ferric ion sequestering agents. 13. Synthesis, structures, and thermodynamics of complexation of cobalt(III) and iron(III) tris complexes of several chelating hydroxypyridinones *Inorg. Chem.*, 1985, **24**, 954-967.
31. B. F. Monzyk and A. L. Crumbliss, Kinetics and mechanism of the stepwise dissociation of iron (III) from ferrioxamine B in aqueous acid, *Journal of the American Chemical Society*, 1982, **104**, 4921-4929.
32. G. Schwarzenbach and K. Schwarzenbach, Hydroxamatkomplexe I. Die Stabilität der Eisen (III)-Komplexe einfacher Hydroxamsäuren und des Ferrioxamins B, *Helvetica Chimica Acta*, 1963, **46**, 1390-1400.
33. M. Birus, N. Kujundzic and M. Pribanic, Kinetics of complexation of iron (III) in aqueous solution, *Progress in reaction kinetics*, 1993, **18**, 171-271.
34. M. T. Caudle and A. L. Crumbliss, Dissociation Kinetics of (N-Methylacetohydroxamato) iron (III) Complexes: A Model for Probing Electronic and Structural Effects in the Dissociation of Siderophore Complexes, *Inorganic Chemistry*, 1994, **33**, 4077-4085.
35. E. Poggiali, E. Cassinerio, L. Zanaboni and M. D. Cappellini, An update on iron chelation therapy, *Blood Transfusion*, 2012, **10**, 411-422.
36. G. Link, A. M. Konijn, W. Breuer, Z. I. Cabantchik and C. Hershko, Exploring the “iron shuttle” hypothesis in chelation therapy: Effects of combined deferoxamine and deferiprone treatment in hypertransfused rats with labeled iron stores and in iron-loaded

<DMHP catalysis paper submitted 1-26-18.docx>

rat heart cells in culture, *Journal of Laboratory and Clinical Medicine*, 2001, **138**, 130-138.

## Table of Contents Entry



Catalysis of iron(III) exchange between two chelators by a bidentate siderophore mimic is discussed in the context of iron homeostasis.